INTERNATIONAL JOURNAL FOR NUMERICAL METHODS IN FLUIDS, VOL. 3, 529–542 (1983)

INCOMPRESSIBLE FLOW IN A RAPIDLY ROTATING CYLINDER WITH A SOURCE/SINK DISTRIBUTION IN THE LATERAL WALL AND A FREE INNER BOUNDARY

ROBERT J. RIBANDO

Department of Mechanical and Aerospace Engineering, School of Engineering and Applied Science, University of Virginia, Charlottesville, Virginia

SUMMARY

The flow of an incompressible fluid in a rapidly rotating right circular cylinder is considered. A source/sink mass distribution at the lateral wall, which is azimuthally uniform and symmetric across the midplane, causes a deviation from wheel flow. The container is only partially full and the inner free surface is allowed to deviate slightly from the vertical. A finite-difference solution of the full axisymmetric, non-linear governing equations was used to obtain the flow field. A special implicit technique for the Coriolis terms which maintains geostrophy was developed and is described. The results obtained for a low Rossby number flow compare quite favourably with the linearized solution. Results are also presented for a case wherein the non-linear terms are important.

KEY WORDS Strongly Rotating Incompressible Free-surface Finite-difference Coriolis

INTRODUCTION

Source–sink flows in a rotating fluid have been considered by a number of authors including Lewellen,[1] Barcilon,[2] Hide,[3] and Wood and Sanders.[4] Lewellen considered a vortex flow in which the fluid entered tangentially with high velocity, spiralled radially inward and exited axially at a smaller radius. Barcilon considered a rotating flow in which the fluid was injected from the sidewall at one height and azimuthal position and removed at a different height and azimuthal position. He found using matching techniques that the vertical transport is confined to a layer of $E^{1/3}$ thickness (E being the Ekman number, $\nu/\Omega L^2$) whereas the horizontal transport is through the interior of the fluid. Hide studied both theoretically and experimentally a number of cases involving coaxial cylinders with sources and sinks in the vertical walls. Wood and Sanders extended the Onsager 'Pancake' model to allow for the presence of sources and sinks of mass, momentum and energy within a rapidly rotating gas.

Considered here is a case involving an incompressible liquid in an annular geometry. The inner surface is nearly vertical and completely free; mass injection and removal takes place through the outer permeable wall. A finite-difference solution of the axisymmetric governing equations is compared to the linearized asymptotic solution. A case involving a much higher mass injection rate, so that non-linear effects become important, is also investigated.

PROBLEM FORMULATION

The region of interest is shown in Figure 1. The right circular cylinder is only partially filled with liquid and is rotating fast enough that the liquid–air interface is nearly vertical. The

0271–2091/83/060529–14$01.40

Received 1 March 1982
Revised 9 July 1982

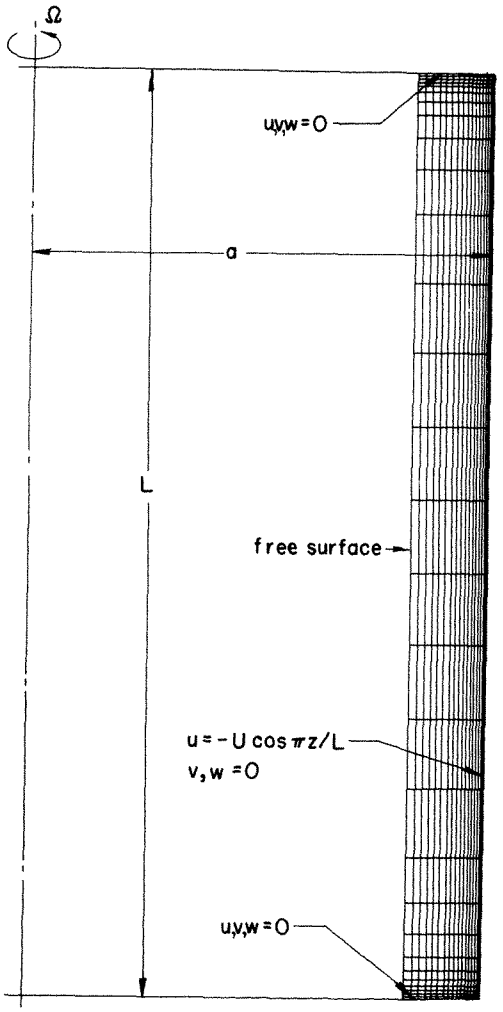

Figure 1. Computing region with finite-difference mesh overlaid

prescribed mass flux through the sidewall is azimuthally uniform and symmetric across the rotor midplane and is given by $u = -U \cos \pi z/L$. The inner surface is a free (slip) surface and is allowed to deviate slightly from the vertical. The horizontal boundaries are no-slip surfaces, as is the sidewall. In Figure 1, the finite-difference mesh (discussed later) is shown covering the liquid-filled region. The axisymmetric governing equations are written as follows:[5]

$$\frac{\partial u}{\partial t} = -\frac{1}{r}\frac{\partial}{\partial r}(ruu) - \frac{\partial}{\partial z}(uw) + \left(2\Omega + \frac{v}{r}\right)v - \frac{1}{\rho_0}\frac{\partial p}{\partial r} + \nu\left[\frac{\partial}{\partial r}\frac{1}{r}\frac{\partial}{\partial r}(ru) + \frac{\partial^2 u}{\partial z^2}\right] \tag{1}$$

$$\frac{\partial v}{\partial t} = -\frac{1}{r}\frac{\partial}{\partial r}(ruv) - \frac{\partial}{\partial z}(vw) - \left(2\Omega + \frac{v}{r}\right)u + \nu\left[\frac{\partial}{\partial r}\frac{1}{r}\frac{\partial}{\partial r}(rv) + \frac{\partial^2 v}{\partial z^2}\right] \tag{2}$$

$$\frac{\partial w}{\partial t} = -\frac{1}{r}\frac{\partial}{\partial r}(ruw) - \frac{\partial}{\partial z}(ww) - \frac{1}{\rho_0}\frac{\partial p}{\partial z} + \nu\left[\frac{1}{r}\frac{\partial}{\partial r}\left(r\frac{\partial w}{\partial r}\right) + \frac{\partial^2 w}{\partial z^2}\right] \tag{3}$$

$$\frac{1}{r}\frac{\partial}{\partial r}(ru) + \frac{\partial w}{\partial z} = 0 \tag{4}$$

The pressure which appears in these equations is the reduced pressure; that is, the actual pressure has been combined with the centrifugal acceleration term.[6]

Gravity has been neglected; for the flows being considered here the ratio of centrifugal to gravitational acceleration is nearly 100. The inclusion of gravity would be trivial so long as the assumption that the deviation of the free surface from vertical is small is still valid.

The solution of Equations (1)–(4) by finite-difference techniques is considered in the next section.

NUMERICAL FORMULATION

Initial solutions of this problem employing a technique similar to that used by Beardsley *et al.*[5] for much less rapidly rotating flows without a free surface exhibited a strong, slowly-damping mode of free-surface oscillation. Occasionally the computed flow would become unstable and break into Taylor-like vortices even though all apparent numerical stability requirements were satisfied. The technique to be presented here virtually eliminated the sloshing mode, eliminated all stability problems and gives an efficient transient or steady state solution for rapidly rotating axisymmetric flows. With one notable exception the primitive variable technique used here is similar to that used by Beardsley *et al.*[5] for rotating flows and by numerous other authors for rotating and non-rotating flows.[7]

The mesh system employed is shown in Figure 2 and the nodalization of the liquid-filled region is shown in Figure 1. Pressure (and when applicable any other state quantities) is defined at the centre of the primary control volumes. The control volumes for radial velocity and the vertical velocity are shifted a half grid space to the right and a half grid space upward, respectively. That is, these auxiliary volumes are centred on the edges of the primary control volume. For a fully three-dimensional flow, the control volume for the azimuthal velocity would normally be taken to be coincident with the primary (pressure) control volume and shifted a half-grid space into the paper. Instead, for reasons that will become apparent later, the control volume for azimuthal velocity is taken to be the same as that for the radial velocity. Although the program based on this formulation uses a non-uniform grid spacing in both directions with nodes concentrated near the ends and next to the sidewall, for ease of discussion the rest of this analysis will be based on a uniform mesh. Looking at the finite differencing in an abbreviated form at present and with

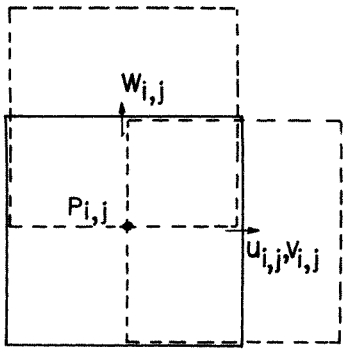

Figure 2. Nodal volumes used for pressure and the three velocity components

superscripts indicating time levels, Equations (1)–(3) are differenced as follows:

$$\frac{u_{i,j}^{N+1}-u_{i,j}^{N}}{\Delta t}=\text{Convection}_{i,j}^{N}+2\Omega v_{i,j}^{N+1}+\text{Curvature}_{i,j}^{N}+\frac{1}{\rho_0}\frac{p_{i,j}^{N+1}-p_{i+1,j}^{N+1}}{\Delta r}+\text{Viscous}_{i,j}^{N} \tag{5}$$

$$\frac{v_{i,j}^{N+1}-v_{i,j}^{N}}{\Delta t}=\text{Convection}_{i,j}^{N}-2\Omega u_{i,j}^{N+1}+\text{Curvature}_{i,j}^{N}+\text{Viscous}_{i,j}^{N}, \tag{6}$$

$$\frac{w_{i,j}^{N+1}-w_{i,j}^{N}}{\Delta t}=\text{Convection}_{i,j}^{N}+\frac{1}{\rho_0}\frac{p_{i,j}^{N+1}-p_{i,j+1}^{N+1}}{\Delta z}+\text{Viscous}_{i,j}^{N} \tag{7}$$

The usual explicit methods, e.g. second central differences and conserving upwind differences[8] are used for the viscous and convection terms, respectively. No attempt was made to mitigate numerical diffusion effects due to upwinding of the convection terms.[9]

Since $u_{i,j}$ and $v_{i,j}$ are evaluated at the same point, Equation (6) may be used to eliminate $v_{i,j}^{N+1}$ in equation (5), leaving an equation containing only the variables $u_{i,j}$ and $p_{i,j}$ at the advanced $(N+1)$ time level. If the radial and azimuthal control volumes had not been taken to be coincident, then in the radial momentum equation, for instance, the term $2\Omega v$ would be evaluated as $\Omega(v_{i+\frac{1}{2},j}+v_{i-\frac{1}{2},j})$ as in Beardsley.[5] The simple substitution used here would not have been possible.

Requiring continuity to be satisfied at the new time level (and ignoring curvature effects only for purposes of this discussion), equation (4) in difference form becomes:

$$u_{i-1,j}^{N+1}\Delta z-u_{i,j}^{N+1}\Delta z+w_{i,j-1}^{N+1}\Delta r-w_{i,j}^{N+1}\Delta r=0 \tag{8}$$

Equation (5), with $v_{i,j}^{N+1}$ eliminated by the substitution discussed, an analogous expression for $u_{i-1,j}^{N+1}$, equation (7) for $w_{i,j}^{N+1}$ and an analogous expression for $w_{i,j-1}^{N+1}$ are substituted into equation (8) to obtain an equation involving pressure at the grid point and its four neighbours at the new time level. This Poisson equation for pressure is solved using cyclic reduction.[10]

The computational sequence then is as follows:

1. Update explicit terms (convection, viscous, curvature) in equations (5)–(7).
2. Substitute equation (6) into (5) and solve for $u_{i,j}^{N+1}$.
3. Substitute equation (7) and the modified equation (5) and their counterparts at $w_{i,j-1}$ and $u_{i-1,j}$ into equation (8).
4. Solve resulting Poisson equation for pressure.
5. Update all velocities using new pressure field.
6. Update all explicit boundary conditions.
7. Repeat 1–6 until convergence.

Note that by the simple expedient of defining identical control volumes for the radial and azimuthal velocities, it is possible in an axisymmetric flow to treat the Coriolis terms fully implicitly rather than explicitly as done by Beardsley *et al.*[5] and others.[11] Also all terms in that subset of the full governing equations which describe inviscid inertial waves[6] have been treated implicitly. Thus the present treatment of inertial waves is exactly analogous to the treatment of acoustic waves in the ICE (implicit continuous-fluid Eulerian) technique[12] for compressible and incompressible fluids. Analogous benefits in terms of allowable time step and absence of truncation error-induced waves may be expected. A recent paper by Hirt and Nichols[13] discusses the treatment of acoustic waves in a simple one-dimensional geometry and shows conclusively the advantages of implicit over explicit treatment.

Note that the technique described here is directly applicable only to axisymmetric flows.

Flows involving high enough angular frequencies that the time step restriction due to explicit treatment of the Coriolis terms is a problem would more than likely be axisymmetric anyway. Such flows arise, for instance, in centrifuges.

One other, less important difference between the current treatment and that of Beardsley *et al.*[5] involves the finite-differencing of the first viscous term in equation (2). The current analysis uses instead the form,

$$\frac{1}{r^2}\frac{\partial}{\partial r} r^3 \frac{\partial v/r}{\partial r} \tag{9}$$

which arises directly from first principles[14] and reduces, of course, to the form appearing in equation (2). In the form used here, the finite-difference approximation to the tangential shear stress is identically zero for the condition of wheel flow, as it should be. Further, the no-shear stress condition at the free inner boundary may be applied with no ambiguity.

To complete the formulation, boundary conditions must be prescribed. At the lateral wall the radial velocity is prescribed for all time. For the row of nodes along the wall this known value is used instead of equation (5) for $u_{i,j}^{N+1}$ in equation (8). Thus a four-point form of the Poisson equation is used at nodes adjacent to the sidewall. The no-slip condition for the axial velocity at this wall is enforced through simple reflection (with sign change) during the explicit update of the diffusion terms. The azimuthal velocity, which is defined at the wall rather than a half grid space off as is the vertical, is identically zero at the wall.

Several options are available at the horizontal surfaces. For large enough Ekman number, the Ekman boundary layer may be resolved numerically. That is, the vertical mesh may be refined at the ends and the no-slip condition may be applied directly. This option would become more attractive were an explicit, unconditionally stable method such as the DuFort–Frankel method[15] employed for diffusion terms. If the option of grid refinement and resolution is used, then the axial velocity, which is defined exactly at the wall, is identically zero. The no-slip condition for the radial and azimuthal velocities, which are defined a half space out from the horizontal walls, is applied through a simple reflection with sign change. For the flows considered in this paper the Ekman layers are such that an analytical 'patch' becomes more reasonable. That is, a boundary condition which has the equivalent effect on the main flow as a no-slip condition is used instead of the no-slip condition itself. In this case, the end boundary condition becomes one on axial velocity and is expressed in terms of the azimuthal velocity outside the Ekman layer:[6]

$$w = -\tfrac{1}{2}E^{1/2}\hat{\mathbf{k}}\cdot\nabla\times\mathbf{q} = -\tfrac{1}{2}E^{1/2}\frac{1}{r}\frac{\partial}{\partial r} rv \quad \text{at} \quad z = z_{\text{top}} \tag{10}$$

and

$$w = +\tfrac{1}{2}E^{1/2}\hat{\mathbf{k}}\cdot\nabla\times\mathbf{q} = +\tfrac{1}{2}E^{1/2}\frac{1}{r}\frac{\partial}{\partial r} rv \quad \text{at} \quad z = z_{\text{bottom}} \tag{11}$$

The Ekman flow has been evaluated explicitly, that is, $w^{N+1} = f(v^N)$. A fully implicit treatment of the Ekman suction flow would result in a Poisson equation for pressure which is not separable, since at the ends the axial flow would depend on a horizontal pressure gradient (the azimuthal flow being strongly coupled to the radial flow) rather than on a vertical pressure gradient as in the rest of the field. The non-separable equation would be somewhat more difficult to solve than the present separable one. The explicit treatment has been found to be adequate; for the case in question we expect from the linearized analysis that the Ekman flow will be inconsequential anyway. Because the program is also being used

for cases where the Ekman layers may be economically resolved, axial diffusion terms are retained. When using the analytical end conditions being applied here, a slip condition is applied at either end.

To be more specific, consider the row of cells along the lower boundary. The lower face of this row of cells represents the outer edge of the Ekman layer. The axial flow through the lower edge is computed using equation (11) where the values of the azimuthal velocity appearing on the right hand side are the 'interior' values, which are defined a half grid space above the lower edge (Figure 2). These interior values of azimuthal velocity are computed in the normal way except that here and in the radial momentum equation (equation (1)) the shear stresses acting on the lower faces, which involve axial derivatives, are negated by applying a slip condition; the effect of the 'no-slip' condition having already been incorporated through the compatibility equation (equation (11)). The use of equations (10) and (11) for the non-full cylinder itself creates a problem. In finite-differencing these equations we note that at all internal nodes the term coming from the right side of one cell is equal and opposite to the term coming from the left side of the node to its right and that the extra terms which do not cancel at the ends are zero anyway for the fully-filled cylinder with a no-slip outer wall. This cancellation ensures that at all times the mass going into the Ekman layer is identical to that leaving it. With the stress-free inner boundary employed here, the term-by-term cancellation at nodes away from the wall and the free surface still holds, the azimuthal velocity at the wall is still zero, but the term which comes from the left side of the node abutting the free surface is not zero. Recent work by Shadday[16] and Greenspan[17] on strongly rotating flows involving an inner free surface suggests that for such a case the basic Ekman layer structure is unaltered except to provide at the free surface an extra source of mass which in a completely-full cylinder would have been transported by an upwelling distributed through the inviscid interior from the radius of the free surface into the centreline. For our purposes here we cancel the (small) non-cancelling term in evaluating equations (10) and (11), so that the mass into and out of each Ekman layer balances. In a future paper we will consider a flow in which the Ekman layers provide all the drive and for which both experimental data (LDV measurements) and finite-difference solutions which fully resolve the Ekman layer have recently become available.[16]

The assumption that the deviation of the free surface from vertical is small, but non-zero, has been made. This allows a fairly simple, but adequate treatment of the inner boundary. Since the governing equations have been written in terms of the reduced pressure,[6] then the dominant restoring force is approximately $-\rho r_{\text{nominal}}\Omega^2\eta(z, t)$, where η is the small deviation of the free surface from the nominal vertical position. This restoring force may be incorporated into the finite-difference radial force balances for the column of half-cells along the free boundary in either of two ways. It may be used either as a 'body force' with the condition that $p = 0$ at the nominal position retained, or the pressure at the nominal position may be adjusted to a non-zero value reflecting this force. The former was in fact done. Velocities were also reflected to satisfy the no-stress condition. In the case of the azimuthal velocity the appropriate prescription for reflection comes from equation (9), that is $\tau_{r\theta} = r\dfrac{\partial v/r}{\partial r} = 0$, or $v/r = \text{constant}$.

All dimensions of the free surface cells as they appear in facial areas, volumes etc., were held constant. For stability reasons the restoring force must be evaluated partially at the advanced time level. Noting that the radial velocity of the free surface; that is, $\partial\eta/\partial t$, is identical to the normal velocity of the fluid at the edge nodes, such an implicit treatment becomes straightforward. In short, the cells along the free surface are treated in a similar

fashion to the interior cells, except that they are half-sized, have zero shear stress on the inner face, and have the implicitly treated restoring force. The present treatment does allow surface waves. The computed free surface velocities are typically three to five orders of magnitude less than the mass influx velocity and are decaying with time.

With the usual explicit treatment of the Coriolis terms and with the parameters used in the first of the two cases to be discussed, the most limiting time step restriction is given by $\Delta t \leq 1/2\Omega$.[5] Instead, with the fully implicit treatment of the Coriolis terms used here, the above time step restriction no longer applies, and the most restrictive limitation comes from the fully explicit treatment of the diffusion terms. With the parameters chosen, the time step was about 0·01 s. In the second calculational example, where non-linear effects are important, the maximum allowable time step is[18]

$$\Delta t < \min\left\{\frac{\Delta r}{|u|}, \frac{\Delta z}{|w|}\right\}, \tag{12}$$

which is nearly an order of magnitude smaller.

RESULTS

Two cases are discussed in this study; a low Rossby number flow for which the computed results may be compared to an available linearized solution and a higher Rossby number, non-linear case. Some of the parameters used in this study come from an ongoing, related project in which a non-wheel flow component is driven in a partially-filled rotor by a differentially-rotating lid.[16] These parameters include the rotor dimensions (length = 0·20 m, radius = 0·10 m), the fill ratio (=0·30 by volume), the fluid (water, $\nu = 10^{-6}$ m^2/s) and the rotor speed (=1000 rev/min, $\Omega = 105$ s^{-1}). No experimental work involving the source–sink flow studied herein is currently ongoing, hence the flow through the sidewall was chosen as $U = 0{\cdot}0001 \cos \pi Z/L$ m/s for the first case, and a value 1000 times larger was used for the second case. The shape was picked to simplify the linearized analysis. With these parameters $E = \nu/\Omega L^2 = 2{\cdot}38 \times 10^{-7}$ and the Rossby number ($=U/\Omega L$) based on the amplitude of the injected sidewall flow was $4{\cdot}7 \times 10^{-6}$ for the first case and $4{\cdot}7 \times 10^{-3}$ for the second case. It will be shown later that actual velocities internal to the flow are very much larger than the scaling velocity used.

ANALYTICAL SOLUTION

A solution of this problem using linear theory has been given by Greenspan.[19] According to linear theory the transport is accomplished entirely by a recirculating flow within the sidewall boundary layer. The rigid rotation of the main body of fluid is undisturbed.

Let the cylinder of height L, and radius a, rotate with angular velocity Ω. Assume that at the sidewall, the normal (radial) velocity is prescribed by

$$u = -U \cos \pi z/L$$

so that there is a mass flux into the cylinder below $z = L/2$ and an efflux above. All other boundary conditions are as described earlier; i.e. the horizontal surfaces are no-slip, the sidewall is no-slip and the inner boundary is stress-free.

With $\gamma = (2\pi/E)^{1/3}$ and $x = a - r$, an asymptotic analysis,[6] yields the following for the axial and azimuthal velocity components:

$$\tilde{w} = A(x) \sin(\pi z/L)$$

$$\tilde{v} = A(x) \cos(\pi z/L)$$

where

$$A(x) = \frac{2\gamma}{\pi\sqrt{3}} Ue^{-((\gamma/2)(x/L))} \sin\left(\frac{\sqrt{3}\gamma}{2}\frac{x}{L}\right)$$

Both components are large, i.e. Order $(E^{-1/3}U)$ or about 160 U in this case, and alternate in direction from the wall.

The above expression for axial velocity was evaluated for each node on the finite difference mesh and the resulting velocity field was integrated to obtain the streamfield. The result is presented in Figure 3. The radial co-ordinate has been expanded by a factor of 10 and streamlines are plotted in increments of 10 per cent of the total flow injected through the sidewall. The left edge of the plot is the free surface, not the rotor centreline. The sinusoidal dependence of axial velocity on distance from the wall is evidenced by the counter-rotating cells to the left of the dividing streamline. It can be seen that the flow in the left two-thirds of the region was low enough that no non-zero streamlines were found although increasingly weaker cells are in fact there. In Figure 4, contours of constant

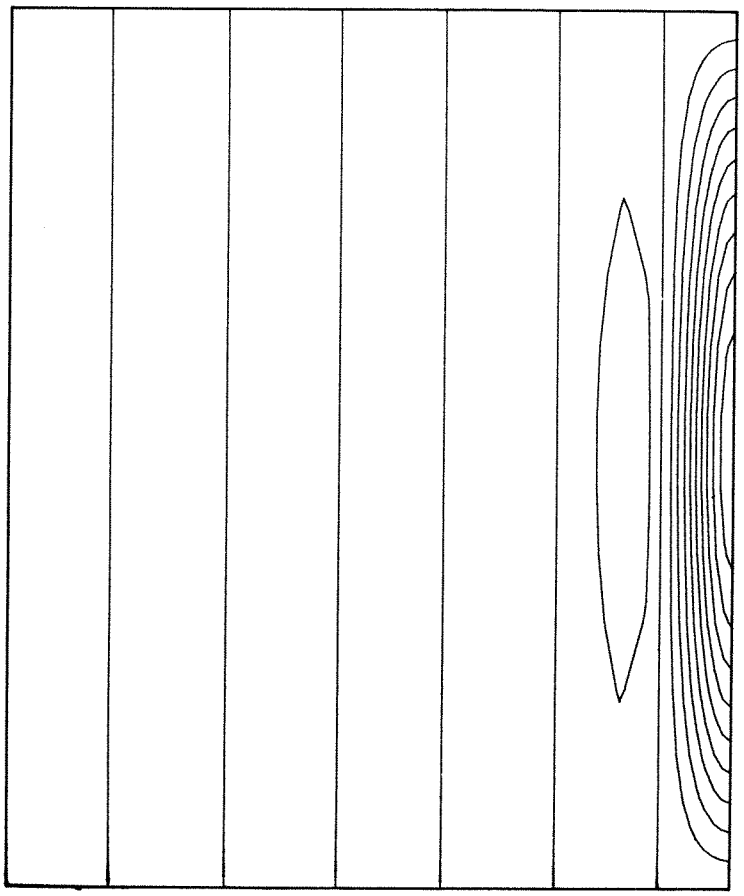

Figure 3. Streamlines computed from Greenspan's linearized solution. Streamline increment is 10 per cent of the inflow through the sidewall. In this plot and all succeeding plots the horizontal co-ordinate has been expanded by a factor of 10 and the left edge is the free surface. $E = 2{\cdot}38 \times 10^{-7}$

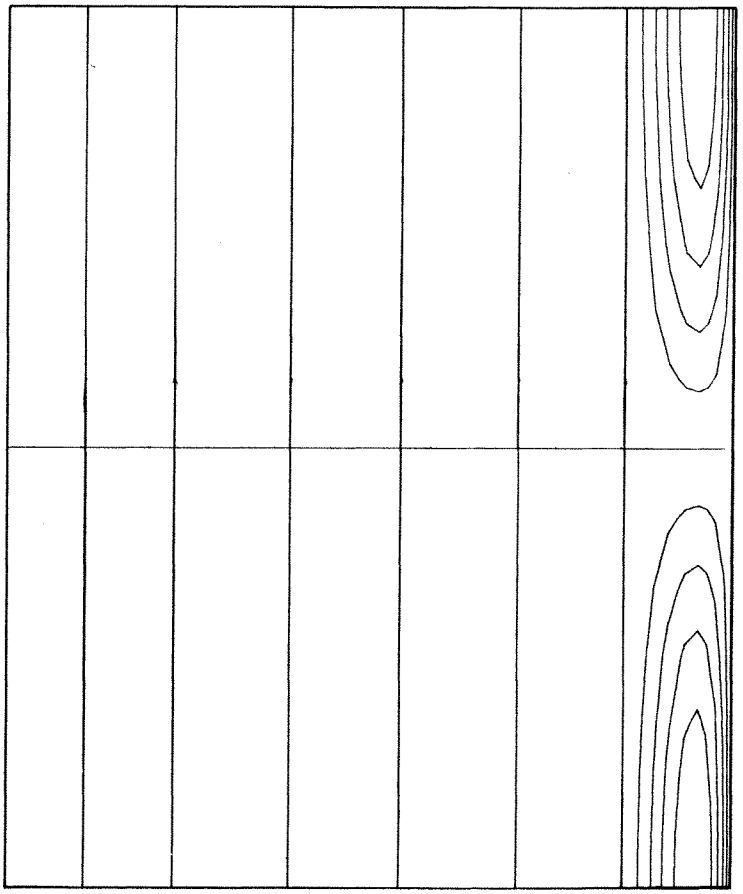

Figure 4. Contours of constant azimuthal velocity for flow of Figure 3. The contour interval is 10 per cent of the difference between the maximum and minimum values. ($v_{max} = -v_{min} = 51 \times U$)

azimuthal velocity have been plotted. The flow entering in the lower half immediately gains angular velocity; that leaving has a deficit which must be eliminated before exiting. With the negative exponential dependence on distance from the wall, only zero contours are found in most of the flow. In the linear solution the maximum azimuthal velocity was found to be 51 times the maximum inflow velocity.

NUMERICAL SOLUTION

The steady state flow field obtained using the transient finite-difference technique discussed earlier with the lower value of the inflow velocity ($U = 0{\cdot}0001 \cos \pi z/L$ m/s) is shown in Figures 5 and 6. A 20×31 mesh (Figure 1) was employed. The streamlines shown in Figure 5 were obtained by integrating the computed vertical velocity components. As in Figure 3 the streamline increment is 10 per cent of the inflow through the sidewall and the horizontal co-ordinate has been expanded by a factor of 10. Again the left edge of the plot is the free surface, not the rotor centreline. With wheel flow initial conditions, the sidewall flow was

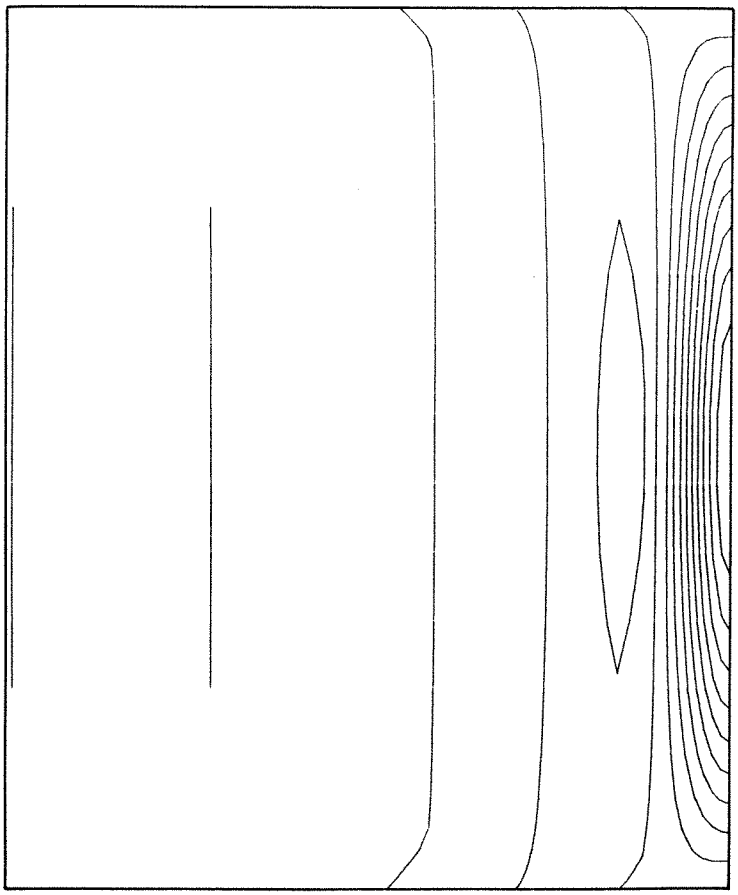

Figure 5. Streamlines computed using finite-difference method for low Rossby number case. Streamline increment is 10 per cent of the inflow through the sidewall. $E = 2{\cdot}38 \times 10^{-7}$, $Ro = 4{\cdot}7 \times 10^{-6}$

ramped up to its final value in one second (~17 revolutions). The calculation was considered converged when at a time of 7·3 s the largest change in pressure at any grid point between successive timesteps normalized by the largest pressure in the field was less than 0·005 per cent. (For the parameters used in this study, this time is the same order as the spin-up time scale.) The flow to the right of the dividing streamline reached virtually its final distribution almost at the end of the one-second ramp. Weak secondary cells grew and decayed during the rest of the transient. Very weak free surface oscillations still existed at the end of the run; the final deviation of the free surface from the vertical is infinitesimal (order 10^{-9} m). In general, agreement between the linearized and numerical solutions is seen to be quite good. Slight differences in the position of the series of zero streamlines to the left is certainly expected given the coarseness of the finite-difference mesh used there and the very small magnitude of the flow there. In some cases, only one or possibly two grid points span an entire cell. The evaluation of the linearized solution was also made on the same mesh, so in

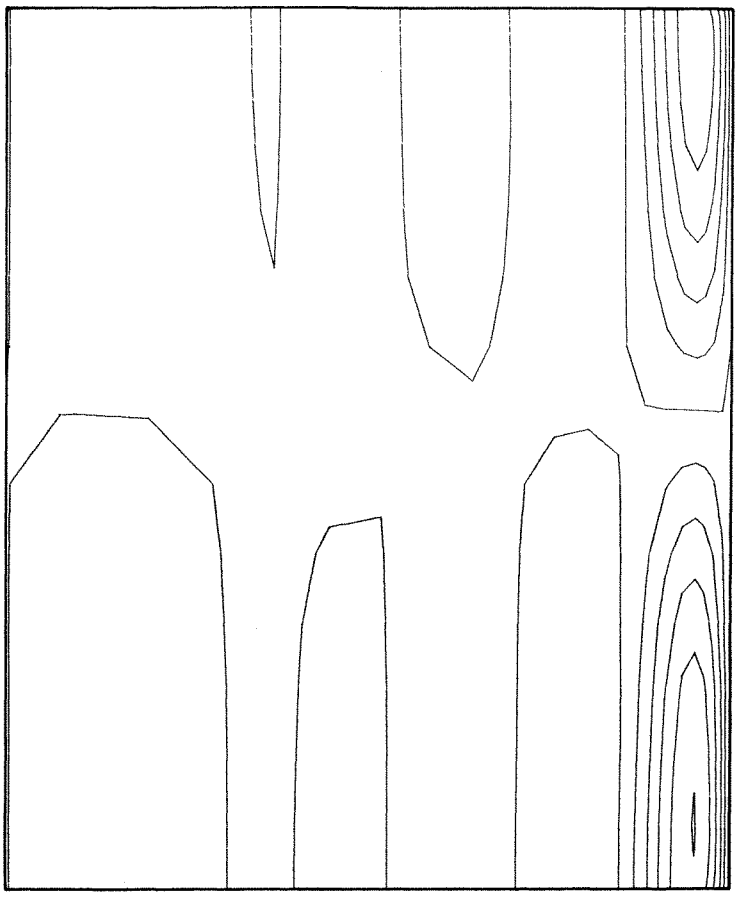

Figure 6. Contours of constant azimuthal velocity for flow of Figure 5. Contour interval is 10 per cent of the difference between the maximum and minimum values ($v_{max} = 48 \times U$)

fact, both solutions are suspect. The negligibility of the non-linear terms for these parameters is surely confirmed.

In Figure 6 contours of constant azimuthal velocity have been plotted. Other than the zero values in the third of the flow near the free surface, the agreement between Figure 4 and Figure 6 is quite close. The maximum azimuthal velocity was found to be 48 times the amplitude of the sidewall inflow, a ratio very close to that determined from Greenspan's solution. Total computer time for this case was 590 s on a CDC Cyber 730.

With the inflow velocity raised by a factor of 1000; i.e. $U = 0{\cdot}1 \cos \pi z/L$ m/s, the character of the flow is markedly different. Figures 7 and 8 show the computed streamlines and lines of constant azimuthal velocity for this non-linear case. Again the flow was ramped in over a period of one second, and the calculation was terminated at 1·7 s when the largest change in pressure at any grid point between successive timesteps normalized by the highest pressure in the flow was less than 0·05 per cent. Using equation (12) as a criterion, the allowable timestep was reduced from that used in the nearly-linear case by a factor of about 10. At

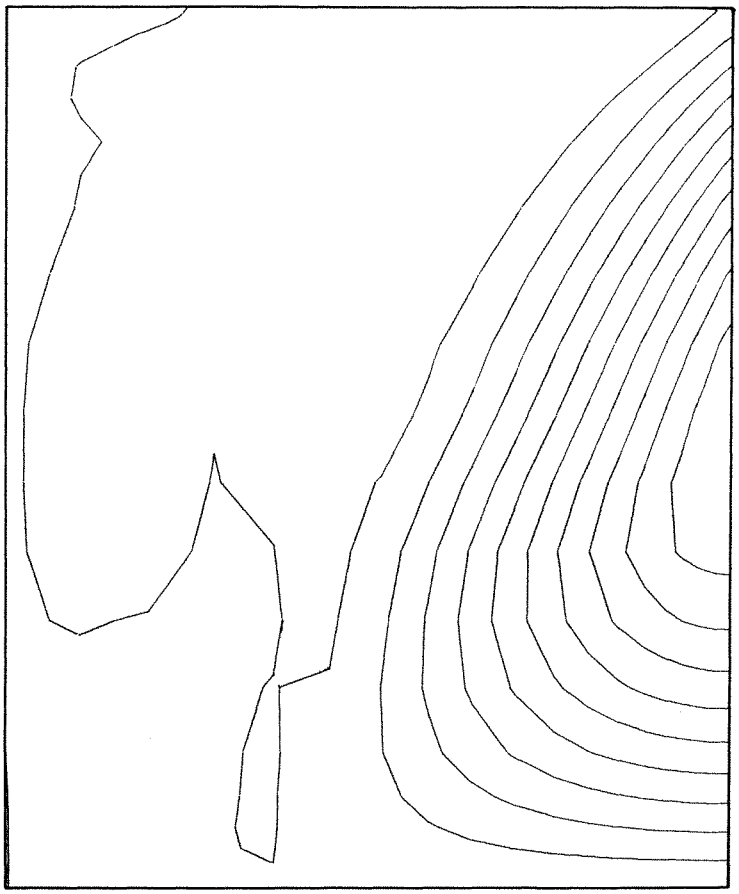

Figure 7. Streamlines computed using finite-difference method for higher Rossby number case. Streamline increment is 10 per cent of the inflow through the sidewall. $E = 2{\cdot}38 \times 10^{-7}$, $Ro = 4{\cdot}7 \times 10^{-3}$

convergence only the zero streamline and the zero contour of azimuthal velocity were still meandering slightly. The flow is no longer symmetric top-to-bottom and the well-ordered secondary structure is gone. The strong wall inflow penetrates much farther into the flow. The maximum azimuthal velocity in this case was about 17 times the inflow amplitude against 48 for the nearly-linear case.

CONCLUSIONS

A finite-difference scheme which is applicable to strongly rotating, axisymmetric, incompressible flows has been described. The very strong coupling between the horizontal velocity components has been implicitly treated in the algorithm. A simple treatment has been used for the nearly-vertical free surface. Good agreement between an available asymptotic solution and the computed results for a low Rossby number case has been shown. The robustness of the algorithm at higher Rossby numbers where non-linear effects become important has also been demonstrated.

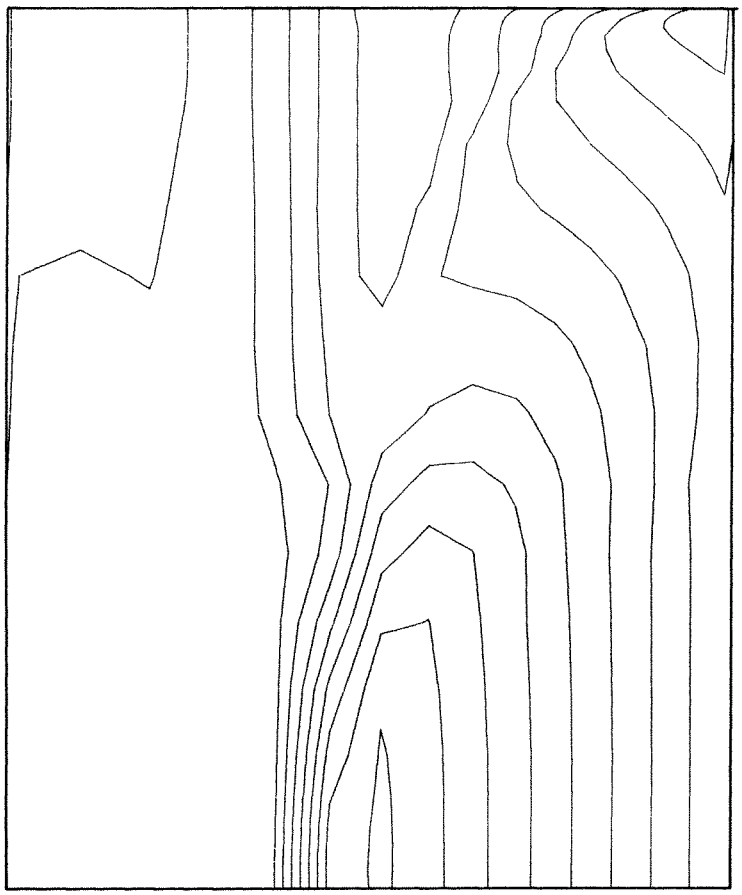

Figure 8. Contours of constant azimuthal velocity corresponding to flow shown in Figure 7. Contour interval is 10 per cent of the difference between the maximum and minimum values ($v_{max} = 17\ U$)

ACKNOWLEDGEMENT

Research supported by the U.S. Department of Energy under Contract No. DE-AC05-820R20900.

REFERENCES

1. W. S. Lewellen, 'A solution for three-dimensional vortex flows with strong circulation', *J. Fluid Mech.*, **14,** 420–432 (1962).
2. V. Barcilon, 'On the motion due to sources and sinks distributed along the vertical boundary of a rotating fluid', *J. Fluid Mech.*, **27,** 551–560 (1967).
3. R. Hide, 'On source–sink flows in a rotating fluid', *J. Fluid Mech.*, **32,** Part 4, 737–764 (1968).
4. H. G. Wood and G. Sanders, 'Rotating compressible flows with internal sources and sinks', accepted for publication in the *J. Fluid Mech.* (1983).
5. R. C. Beardsley, K. D. Saunders, A. C. Warn-Varnas and J. M. Harding, 'An experimental and numerical study of the secular spin-up of a thermally stratified rotating fluid', *J. Fluid Mech.*, **93,** Part 1, 161–184 (1979).
6. H. P. Greenspan, *The Theory of Rotating Fluids,* Cambridge University Press, Cambridge, 1969.
7. F. H. Harlow and J. E. Welch, 'Numerical calculations of time-dependent viscous incompressible flow of fluid with free surface', *Physics of Fluids,* **8,** (12), 2182–2189 (1965).

8. K. E. Torrance, 'Comparison of finite-difference computations of natural convection', *J. of Research of the National Bureau of Standards*, **72B,** (4) 281–301 (1968).
9. J. P. Boris and D. L. Book, 'Flux-corrected transport. 1. Shasta, a fluid transport algorithm that works', *J. Computational Physics*, **11,** 38–69 (1973).
10. R. A. Sweet, 'Direct methods for the solution of Poisson's equation on a staggered grid', *J. Computational Physics*, **12,** 422–428 (1973).
11. G. P. Williams, 'Numerical integration of the three-dimensional Navier–Stokes equations for incompressible flow', *J. Fluid Mech.*, **37,** Part 4, 727–750 (1969).
12. F. H. Harlow and A. A. Amsden, 'A numerical fluid dynamics calculation method for all flow speeds', *J. Computational Physics*, **8,** 197–213 (1971).
13. C. W. Hirt and B. D. Nichols, 'Adding limited compressibility to incompressible hydrocodes', *J. Computational Physics*, **34,** 390–400 (1980).
14. G. K. Batchelor, *An Introduction to Fluid Dynamics*, Cambridge University Press, Cambridge, 1967.
15. P. J. Roache, *Computational Fluid Dynamics*, Hermosa Publishers, Albuquerque, 1976.
16. M. A. Shadday, *Ph.D. Dissertation*, University of Virginia, May 1982.
17. H. P. Greenspan, 'Simulation of countercurrent flow in a gas centrifuge', *UVA-ER-746-82U*, April 1982.
18. C. W. Hirt, B. D. Nichols and N. C. Romero, 'Sola-A numerical solution algorithm for transient fluid flows', Los Alamos National Laboratory, *LA-5852* (1975).
19. H. P. Greenspan, Ltr. to Ralph Lowry, University of Virginia, 1979.